A Single Vector Platform for High-Level Gene Transduction of Central Neurons: Adeno-Associated Virus Vector Equipped with the Tet-Off System.

AUTHOR(S):

Sohn, Jaerin; Takahashi, Megumu; Okamoto, Shinichiro; Ishida, Yoko; Furuta, Takahiro; Hioki, Hiroyuki

CITATION:

Sohn, Jaerin ...[et al]. A Single Vector Platform for High-Level Gene Transduction of Central Neurons: Adeno-Associated Virus Vector Equipped with the Tet-Off System.. PLOS ONE 2017, 12(1): e0169611.

ISSUE DATE:

2017-01-06

URL:

http://hdl.handle.net/2433/217911

PLOS ONE

RESEARCH ARTICLE

A Single Vector Platform for High-Level Gene Transduction of Central Neurons: Adeno-Associated Virus Vector Equipped with the Tet-Off System

Jaerin Sohn[1,2], Megumu Takahashi[1], Shinichiro Okamoto[1], Yoko Ishida[1], Takahiro Furuta[1], Hiroyuki Hioki[1]*

1 Department of Morphological Brain Science, Graduate School of Medicine, Kyoto University, Yoshida-Konoe-cho, Sakyo-ku, Kyoto, Japan, **2** Division of Cerebral Circuitry, National Institute for Physiological Sciences, Higashiyama, Myodaiji-cho, Okazaki, Japan

* hioki@mbs.med.kyoto-u.ac.jp

OPEN ACCESS

Citation: Sohn J, Takahashi M, Okamoto S, Ishida Y, Furuta T, Hioki H (2017) A Single Vector Platform for High-Level Gene Transduction of Central Neurons: Adeno-Associated Virus Vector Equipped with the Tet-Off System. PLoS ONE 12(1): e0169611. doi:10.1371/journal.pone.0169611

Editor: Simone Di Giovanni, University of Tuebingen, GERMANY

Received: September 20, 2016

Accepted: December 19, 2016

Published: January 6, 2017

Data Availability Statement: All relevant data are within the paper and its Supporting Information file.

Funding: This work was supported by Grants-in-Aid from The Ministry of Education, Culture, Sports, Science, and Technology (MEXT) and Japan Society for the Promotion of Science (JSPS); for JSPS Fellows (13J01992 to J.S.); for Research Activity Start-up (16H07425 to J.S.); for Scientific Research (15H04266 to T.F., 16H04663

Abstract

Visualization of neurons is indispensable for the investigation of neuronal circuits in the central nervous system. Virus vectors have been widely used for labeling particular subsets of neurons, and the adeno-associated virus (AAV) vector has gained popularity as a tool for gene transfer. Here, we developed a single AAV vector Tet-Off platform, AAV-SynTetOff, to improve the gene-transduction efficiency, specifically in neurons. The platform is composed of regulator and response elements in a single AAV genome. After infection of Neuro-2a cells with the AAV-SynTetOff vector, the transduction efficiency of green fluorescent protein (GFP) was increased by approximately 2- and 15-fold relative to the conventional AAV vector with the human cytomegalovirus (CMV) or human synapsin I (SYN) promoter, respectively. We then injected the AAV vectors into the mouse neostriatum. GFP expression in the neostriatal neurons infected with the AAV-SynTetOff vector was approximately 40-times higher than that with the CMV or SYN promoter. By adding a membrane-targeting signal to GFP, the axon fibers of neostriatal neurons were clearly visualized. In contrast, by attaching somatodendritic membrane-targeting signals to GFP, axon fiber labeling was mostly suppressed. Furthermore, we prepared the AAV-SynTetOff vector, which simultaneously expressed somatodendritic membrane-targeted GFP and membrane-targeted red fluorescent protein (RFP). After injection of the vector into the neostriatum, the cell bodies and dendrites of neostriatal neurons were labeled with both GFP and RFP, whereas the axons in the projection sites were labeled only with RFP. Finally, we applied this vector to vasoactive intestinal polypeptide-positive (VIP+) neocortical neurons, one of the subclasses of inhibitory neurons in the neocortex, in layer 2/3 of the mouse primary somatosensory cortex. The results revealed the differential distribution of the somatodendritic and axonal structures at the population level. The AAV-SynTetOff vector developed in the present study exhibits strong fluorescence labeling and has promising applications in neuronal imaging.

to H.H.); for Exploratory Research (15K14333 to H. H.); and for Scientific Research on Innovative Areas, "Neuronal Diversity and Neocortical Organization" (25123709 to H.H.), "Adaptive Circuit Shift" (15H01430 to H.H.), and "Resonance Bio" (16H01426 to H.H.).

Competing Interests: The authors have declared that no competing interests exist.

Introduction

Elucidating the principal design of neuronal circuits is fundamental for understanding how the brain works and implements higher-order functions [1–5]. Visualization of neurons is the first key step in dissecting the neuronal circuits, and the Golgi silver-staining technique has made a great contribution in this field [6, 7]. In addition to Golgi staining, anterograde and retrograde neuronal tracers, such as *Phaseolus vulgaris* leucoagglutinin (PHA-L) [8], biocytin [9], horseradish peroxidase (HRP) [10], and cholera toxin B subunit (CTb) [11], have prompted the study of neuronal connections in the central nervous system [12–14]. However, these conventional methods have drawbacks such as allowing only random but not specific visualization and incomplete labeling of the targeted neurons owing to technical limitations.

Genetic engineering techniques have been applied to neuroscience, and have afforded specific and sufficient labeling of neuronal subpopulations [15, 16]. Transgenic animal lines that express fluorescent proteins have been utilized widely for labeling particular subsets of neurons [17, 18]. The *in utero* electroporation technique enables one to perform cell birthday-specific labeling by introducing plasmids that contain sequences of reporter proteins into target areas of the brain [19–21]. Virus vectors have aroused increasing interest in the field of basic and clinical neurosciences, since the vectors can be directly and locally delivered to the brain region of interest [22, 23]. In addition, gene expression can be limited to particular types of neurons in combination with Cre-driver mouse lines [24, 25]. These genetic tools can be used to determine the architecture of neuronal networks.

Adeno-associated virus (AAV) vectors are now widely applied for gene delivery to neuronal cells. They can be easily purified and highly concentrated, and gene-expression by AAV vectors is efficient and persistent without pathology [26–28]. However, when using ubiquitous promoters, including the human cytomegalovirus (CMV) promoter, gene expression was observed not only in neuronal cells but also in glial cells [29, 30]. Although neuron-specific promoters, such as the human synapsin I (SYN) promoter, achieve specific expression in neuronal cells, the expression level was 10-times less than that achieved with the CMV promoter *in vitro* with self-complementary AAV9 vectors [31]. Thus, it is necessary to develop an efficient neuron-specific gene-expression system with AAV vectors.

In our previous studies, we applied the "Tet-Off system" to lentivirus vectors, and succeeded in achieving strong gene transduction, specifically in neuronal cells, *in vivo* [32, 33]. The expression system is composed of two kinds of units: 1) the regulator unit expresses an improved version of tetracycline-controlled transactivator (tTAad), specifically in neurons, *via* the SYN promoter, and 2) the response unit strongly expresses the gene of interest under the tetracycline-responsive element (TRE) promoter, to which tTAad binds. In the present study, we incorporated these two units into the single genome of AAV serotype 2 (AAV2), produced virus particles pseudotyped with the capsid from serotype 1, and demonstrated high-level expression of the reporter protein *in vitro* and *in vivo*.

We further prepared AAV2/1 vectors that express green fluorescent protein (GFP) or monomeric red fluorescent protein (mRFP1) [34] with a membrane-targeting signal, such as palmitoylation and/or myristoylation signals [35–39], and clearly labeled the axon fibers of neostriatal neurons. By fusing a dendritic membrane-targeting signal to GFP [39, 40], we visualized the cell bodies and dendrites of the infected cells but not the axonal structures. Finally, we generated the AAV2/1 vector that expresses both somatodendritic membrane-targeted GFP and membrane-targeted mRFP1 in the presence of Cre recombinase, and quantitatively analyzed the dendritic and axonal distributions of vasoactive intestinal polypeptide-positive (VIP+) inhibitory neurons into layer (L) 2/3 of the mouse primary somatosensory cortex barrel field (S1BF).

Materials and Methods

Animals

All animal experiments were conducted in accordance with the National Institutes of Health Guide for the Care and Use of Laboratory Animals, and the experiments were approved by the Committee for Animal Care and Use (MedKyo 15012 and MedKyo 16573) and the Committee for Recombinant DNA Study (120093 and 141008) of Kyoto University. Adult male C57BL/6J mice (Japan SLC, Hamamatsu, Japan) and male Vip$^{tm1(cre)Zjh}$/J (VIP-Cre) mice (The Jackson Laboratory, Bar Harbor, ME; stock number 010908; 2–3 months old) [24] were used in the present study. All efforts were made to minimize animal suffering and the number of animals used.

Plasmid construction for AAV vectors

We amplified the human CMV promoter (nucleotides 1–589 in GenBank U57609.1; primer set P1/P2) or the human SYN promoter (nucleotides 1889–2289 in GenBank accession no. M55301.1; primer set P3/P4 in S1 Table) [41], GFP (primer set P5/P6), and a polyadenylation signal derived from the bovine growth hormone gene (BGHpA; nucleotides 1771–1995 in GenBank AH009106.2; primer set P7/P8) by polymerase chain reaction (PCR). We then inserted the PCR products into the *Hinc*II, *Eco*RV, and *EcoRI*/*BamH*I sites of pBluescript II SK (+) (pBSIISK; Stratagene, La Jolla, CA), respectively, resulting in pBSIISK-CMV-GFP-BGHpA or pBSIISK-SYN-GFP-BGHpA. The sequence of the SYN promoter mostly corresponds to the commonly used one with other virus vectors such as the adenovirus vector [42, 43]. To generate a Gateway entry vector, the *Xho*I-to-*BamH*I fragment from the two plasmids were complementarily inserted into the *BamHI*/*Xho*I sites of pENTR™1A (Life Technologies, Carlsbad, CA), resulting in pENTR1A-CMV-GFP-BGHpA(r) or pBSIISK-SYN-GFP-BGHpA(r). We newly prepared destination vectors, pAAV2-DEST(f) and pAAV2-DEST(r), by amplifying the sequence of R1-ccdB-R2 (primer set P9/P10 and P11/P12) from pLenti6 (Life Technologies) and by inserting the fragment into the *Mul*I/*Pma*CI sites of pAAV-MCS (Stratagene). Then, the inserts from the two entry vectors were transferred to the destination vector pAAV2-DEST(r) by homologous recombination with LR clonase II (Life Technologies), resulting in pAAV2-CMV-GFP-BGHpA and pAAV2-SYN-GFP-BGHpA.

In the previous study, we inserted the SYN promoter, tTAad (Clontech, Palo Alto, CA) and BGHpA (amplified by PCR) into pBSIISK, resulting in pBSIISK-SYN-tTAad-BGHpA [32]. GFP and BGHpA (amplified by PCR) were subcloned into pTRE-Tight (Clontech), and the resulting constructs were named as pTRE-GFP-BGHpA [32]. In the present study, we prepared new vectors by modifying these two plasmids as follows. A polyadenylation signal of Simian virus 40 late (SV40LpA) was amplified by PCR (primer set P13/P14), and was replaced with BGHpA in pBSIISK-SYN-tTAad-BGHpA through the *Bgl*II/*Not*I sites, resulting in pBSIISK-SYN-tTAad-SV40LpA. The insulator sequence [44] was inserted into the *BamHI*/*Xho*I sites of pENTR™1A (primer set P15/P16), and the resulting construct was named as pENTR1A-insulator. The fragment SYN-tTAad-SV40LpA was amplified by PCR (primer set P17/P18), and then complementarily inserted into pENTR1A-insulator between the *BamHI*/*Sal*I sites, resulting in pENTR1A-SV40LpA-tTAad-SYN-insulator. The fragment TRE-GFP-BGHpA [32] was inserted into the *Xho*I/*Not*I sites of pENTR1A-SV40LpA-tTAad-SYN-insulator, resulting in pENTR1A-SV40LpA-tTAad-SYN-insulator-TRE-GFP-BGHpA.

Through the *BamHI*/*Mlu*I sites in this entry vector, the GFP sequence was replaced with the following sequences of reporter proteins: 1) GFP with a palmitoylation signal derived from GAP-43 N-terminus (palGFP) (primer set P19/20) [32, 35–39]; 2) GFP with a myristoylation/palmitoylation signal derived from Fyn N-terminus (myrGFP) (primer set P21/20) [39, 40]; or 3) myrGFP with a somatodendritic-targeting signal, the C-terminal cytoplasmic domain of

low-density lipoprotein receptor (LDLRct), which was originally named as myrGFP-LDLRct in the previous reports (primer set P21/P22) [39, 40], but referred to as FGL in the present study. By using an LR recombination reaction with these entry vectors and a destination vector, pAAV2-DEST(f), we produced pAAV2-SynTetOff-GFP, pAAV2-SynTetOff-palGFP, pAAV2-SynTetOff-myrGFP, and pAAV2-SynTetOff-FGL.

We also prepared a new reporter protein that contained both FGL and mRFP1 [45] tagged with a palmitoylation signal derived from GAP-43 N-terminus (palmRFP1) by overlap PCR as follows: 1) the FGL sequence was amplified with the addition of a furin cleavage site and a 2A self-processing sequence (F2A) [46] to the 3′-terminus (primer set P21/P23); 2) the sequence of palmRFP1 was amplified with the addition of the F2A sequence to the 5′-terminus (primer set P24/P25); and 3) the FGL-2A-palmRFP1 sequence was finally amplified (primer set P21/P25). The PCR products were inserted into pENTR1A-SV40LpA-tTAad-SYN-insulator-TRE-GFP-BGHpA through the *BamH*I/*Mlu*I sites. After an LR recombination reaction with the entry vector and a destination vector, pAAV2-DEST(f), we obtained pAAV2-SynTetOff-FGL-2A-palmRFP1.

For specific gene expression under Cre exposure, we used the flip-excision (FLEX) switch [47]. The switch sequence, composed of two pairs of *loxP* and *lox2272* sites in opposite orientations, was synthesized *de novo* (S1 Table; GenScript, Piscataway, NJ) and inserted into pBSIISK through the *Kpn*I/*Sac*I sites, and the resulting plasmid was named as pBSIISK-hFLEX. Then, the sequence of FGL-2A-palmRFP1 was amplified by PCR (primer set P26/P27), and was inserted into pBSIISK-hFLEX through the *Eco*RI/*Sal*I sites, resulting in pBSIISK-FLEX-FGL-2A-palmRFP1. The GFP sequence of pENTR1A-SV40LpA-tTAad-SYN-insulator-TRE-GFP-BGHpA was replaced with the fragment FLEX-FGL-2A-palmRFP1 through the *BamH*I/*Mlu*I sites. The entry vector was finally converted to pAAV2-SynTetOff-FLEX-FGL-2A-palmRFP1 by an LR recombination reaction with pAAV2-DEST(f).

Production and purification of AAV vectors

pAAVs and two helper plasmids were used for AAV production. pHelper (Stratagene) expresses the adenovirus helper functions (*E2A*, *E4*, and *VA* genes). The other helper plasmid, pBSIISK-R2C1, expressing the replication protein of AAV serotype 2 (Rep2) and the capsid protein of AAV serotype 1 (Cap1), was newly prepared by inserting the following fusion sequences into the *Xho*I/*Not*I sites of pBSIISK: 1) nucleotides 146–2,202 of wild-type AAV2 genome (GenBank accession number, AF043303.1); 2) nucleotides 2,223–4,433 of AAV1 (AF063497.1); and 3) nucleotides 4,438–4,534 of AAV2.

Production and purification of AAV vectors were performed as reported previously [48–50]. Briefly, pAAVs, pHelper, and pBSIISK-R2C1 were cotransfected into HEK293T cells (RCB2202, Riken, Japan) by using polyethylenimine (23966; Polysciences, Inc., Warrington, PA). The medium was replaced 6 h after transfection with Dulbecco's modified Eagle's medium (11965–092; Life Technologies) containing 10% fetal bovine serum, 4 mM L-glutamine (25030–081; Life Technologies), 2 mM GlutaMAX™ (35050–061; Life Technologies), 0.1 M non-essential amino acids (35050–061; Life Technologies), and 1 mM sodium pyruvate (11360–070; Life Technologies). Cells containing virus particles were collected 72 h after medium replacement. After extraction by three cycles of freeze-and-thaw, the virus particles were purified from a crude lysate of the cells by ultracentrifugation with OptiPrep (AXS-1114542; Axis-Shield, Oslo, Norway) and then concentrated by ultrafiltration with Amicon Ultra-15 Centrifugal Filter Unit with Ultracel-50 membrane (UFC905024; Merck Millipore, Darmstadt, Germany).

We added 4 μL of the virus solution into the HEK293T cells on CELLSTAR® cell culture 12-well plates (665180; Greiner Bio-One, Frickenhausen, Germany) in 1 mL of Dulbecco's

modified Eagle's medium containing 10% fetal bovine serum, 2 mM L-glutamine, and 0.1 M non-essential amino acids. After two days of incubation, the genomic DNA of each AAV vector was extracted from the infected cells with QIAamp DNA Mini Kit (51304; QIAGEN, Hombrechtikon, Switzerland). Quantitative PCR (qPCR) was performed on a Mini Opticon Real Time PCR System (Bio-Rad, Hercules, CA) with Ssofast™ EvaGreen supermix (Bio-Rad) (primer set P28/P29). After 40 amplification cycles with an anneal/extension step at 60˚C, the copy number of BGHpA was determined by comparison with the standard curve *via* the Opticon Monitor Software (Bio-Rad), and virus titers (infectious unit/mL, IFU/mL) were adjusted to 1.0×10^{11} IFU/mL with Dulbecco's phosphate-buffered saline (14249–95; Nacalai tesque, Kyoto, Japan). The virus solution was stored in aliquots at −80˚C until use for delivery to brain tissues.

Quantification of GFP expression level in Neuro-2a cells

A Neuro-2a cell line (IFO50081; Health Science Research Resources Bank, Osaka, Japan), derived from mouse albino neuroblastoma, was used for the quantification of GFP expression level *in vitro*. Neuro-2a cells were harvested on CELLSTAR® cell culture 12-well plates in 1 mL of minimum essential medium (11095–080; Life Technologies) with 10% fetal bovine serum and 0.1 M non-essential amino acids solution, and 4 μL of virus solution was then added to each well. After 1-week of incubation in three wells with each virus solution, total RNA and DNA were extracted using an AllPrep DNA/RNA Mini Kit (80204; QIAGEN) according to the manufacturer's protocol. The total RNA and DNA were eluted in 50 and 100 μL of RNase-free water, and 1 and 2 μL were immediately used for analysis, respectively.

Quantitative reverse transcription PCR (qRT-PCR) and qPCR were performed on a Mini Opticon Real Time PCR System with iTaq™ Universal SYBR® Green One-Step Kit (172–5150; Bio-Rad) and Ssofast™ EvaGreen supermix (172–5200; Bio-Rad), respectively, according to the manufacturer's instructions (primer set P30/P31). After 40 amplification cycles with an anneal/extension step at 65˚C for five samples of each AAV vector, we calculated the copy number of GFP in each reaction by comparison with the standard curve *via* the Opticon Monitor Software. The control reactions without template were included in each assay. The GFP-mRNA/GFP-DNA ratio was used as an index of transcriptional activity.

For comparison of GFP-native fluorescence (NF) intensities by infection with AAV vectors, Neuro-2a cells were cultured on Biocoat™ Poly-D-Lysine cover glasses (354087; Corning Life Science, Tewksbury, MA) in the same medium as above, and were incubated for 1 week with 4 μL of virus solutions. The glasses were then removed and fixed with 4% formaldehyde, 0.9% picric acid, and 0.1 M Na_2HPO_4 (adjusted to pH 7.0 with NaOH). After washes with phosphate-buffered 0.9% (w/v) saline (PBS; pH 7.4), the glasses were placed upside down on gelatin-coated glass slides with 50% (v/v) glycerol and 2.5% (w/v) triethylenediamine (anti-fading reagent) in PBS. GFP-native fluorescence (GFP-NF) was observed under a TCS SP8 confocal laser scanning microscope with a 25× water-immersion objective lens (HCX PL APO, NA = 0.95; Leica; ~300 cells in total from three glasses). The digital images were saved as 12-bit TIFF files in gray scale without contrast enhancement. The average intensities per pixel of GFP-NF in cells (arbitrary unit; AU) were measured using ImageJ (ver. 1.48; National Institutes of Health; http://imagej.nih.gov/ij).

Tissue preparation and immunofluorescence staining

The following procedures were performed at room temperature unless stated otherwise. Mice were deeply anesthetized with chloral hydrate (7 mg/10 g body weight) and mounted onto a stereotaxic apparatus. Virus solution (0.2 μL) was injected by pressure through a glass micropipette attached to Picospritzer III (Parker Hannifin Corporation, Cleveland, OH) into the

neostriatum of wild mice (1.0 mm anterior to the bregma, 1.8 mm lateral to the midline, and 2.7–2.8 mm deep from the brain surface) or into the S1BF of VIP-Cre mice (1.0 mm posterior to the bregma, 3.0 mm lateral to the midline, and 0.2–0.3 mm deep from the brain surface). The animals were maintained under regular health checks for 1 week and then subjected to transcardial perfusion as described below.

Mice were deeply anesthetized again with chloral hydrate (7 mg/10 g body weight) and transcardially perfused with PBS. The animals were further perfused with 4% (w/v) formaldehyde, 0.1 M Na_2HPO_4 (adjusted to pH 7.0 with NaOH), and 0.9% (w/v) picric acid. The brains were then removed and postfixed for 3 h in the same fixative. The brain blocks were cut into 40-μm-thick coronal or sagittal sections on a freezing microtome. Virus-injected brain sections were prepared 1 week after the injection.

Brain sections obtained from wild type mice injected with AAV2/1-SynTetOff-FGL-2A-palmRFP1 were incubated overnight in PBS containing 0.3% Triton™ X-100, 0.12% λ-carrageenan, 0.02% sodium azide, and 1% normal donkey serum (PBS-XCD) with 10 μg/mL mouse monoclonal antibody against neuron-specific nuclear protein (NeuN; MAB377; Merck Millipore) or 1 μg/mL rabbit antibody against microtubule-associated protein 2 (MAP2; A0703; Santa Cruz Biotechnology, Santa Cruz, CA). After washes with PBS containing 0.3% Triton™ X-100 (PBS-X), the sections were incubated for 2 h with 5.0 μg/mL Alexa Fluor® 568-conjugated goat antibody against mouse IgG (A-11031; Life Technologies) or 5.0 μg/mL Alexa Fluor® 647-conjugated goat antibody against rabbit IgG (A-21245; Life Technologies) in PBS-XCD. Brain sections obtained from VIP-Cre mice injected with AAV2/1-SynTetOff-FLEX-FGL-2A-palmRFP1 were incubated overnight with a mixture of 20 μg/mL anti-GFP chicken antibody (GFP-1020; Aves Labs, Tigard, OR), 1.0 μg/mL anti-mRFP1 rabbit antibody [51], and 1.0 μg/mL anti-VGluT2 guinea pig antibody [52, 53] in PBS-XCD. After washing, the sections were incubated for 2 h with a mixture of 5 μg/mL Alexa Fluor® 488-conjugated goat antibody against chicken IgY (A-11039; Life Technologies), 5 μg/mL Alexa Fluor® 568-conjugated goat antibody against rabbit IgG (A-11039; Life Technologies), and 5 μg/mL Alexa Fluor® 647-conjugated goat antibody against guinea pig IgG (A-21450; Life Technologies) in PBS-XCD. The sections were finally counterstained with 1 μg/mL DAPI (D-1306; Life Technologies) in PBS-X for identification of cortical layers. The sections were mounted onto gelatin-coated glass slides, and coverslipped with 50% (v/v) glycerol and 2.5% (w/v) triethylenediamine (anti-fading reagent) in PBS.

Image acquisition and measurement of fluorescence intensity

The fluorescence images were acquired under a TCS SP8 confocal laser scanning microscope equipped with a 25× water-immersion objective lens (HCX PL APO, NA = 0.95; Leica) and the pinhole at 1.0 Airy disk unit. GFP and Alexa Fluor® 488, mRFP1 and Alexa Fluor® 568, or Alexa Fluor® 647 was excited with 488, 543, or 633 nm laser beams and observed through 500–580, 590–650, or 660–850 nm emission prism windows, respectively.

The digital images were saved as 12-bit TIFF files in gray scale without contrast enhancement. We measured the average intensities per pixel of GFP-NF in cells (AU) using ImageJ. GFP-NF of ~300 cells from three glasses *in vitro* and that of ~100 neurons in the caudate-putamen (CPu) from three mice were measured for each AAV vector. Cytoarchitecture was determined with reference to NeuN immunoreactivity.

Statistical analysis

Multiple statistical comparisons were performed by Tukey's multiple-comparison test after one-way analysis of variance (Prism4.0c; GraphPad Software, San Diego, CA).

Results

Gene transduction in Neuro-2a cells with AAV-SynTetOff

In this study, we developed a new AAV vector, "AAV-SynTetOff platform" (Fig 1A); the platform is composed of regulator and response elements separated by the chicken β-globin insulator [44] in a single AAV2 genome. The regulator element expressed tTAad under the control of the SYN promoter [41], whereas the response element produced the reporter protein under the TRE promoter, as reported previously for lentivirus vectors [32]. We also prepared AAV vectors expressing GFP under the CMV promoter and the SYN promoter, i.e., AAV2/1-CMV-GFP-BGHpA and AAV2/1-SYN-GFP-BGHpA (Fig 1A), respectively, as control vectors.

One week after infection of Neuro-2a cells with the AAV vectors, we examined the gene-transduction efficiency by assessing the GFP expression level (Fig 1B). After collecting the infected cells, we performed qRT-PCR for GFP-mRNA and qPCR for GFP-DNA, and normalized the expression level of GFP-mRNA by dividing the amount of GFP-DNA. The GFP-mRNA expression was 1.7- or 15.6-fold higher with AAV2/1-SynTetOff-GFP than with AAV2/1-CMV-GFP-BGHpA or AAV2/1-SYN-GFP-BGHpA, respectively (Fig 1C).

We also randomly selected approximately 300 GFP-expressing cells, and measured the average intensity per pixel of GFP-NF in the cell bodies by using the ImageJ software. With AAV2/1-SynTetOff-GFP, the intensity exhibited a 1.8- or 14.4-fold increase compared with AAV2/1-CMV-GFP-BGHpA or AAV2/1-SYN-GFP-BGHpA, respectively (Fig 1C). The increase of GFP-NF intensity was similar to that observed for GFP-mRNA, suggesting that the fluorescence intensity reflects the mRNA expression level.

Strong and neuron-specific gene transduction with AAV-SynTetOff in neostriatal neurons

One week after the injection of the AAV vectors into the mouse neostriatum (caudate-putamen, CPu), we observed strong GFP-NF with AAV2/1-SynTetOff-GFP compared with AAV2/1-CMV-GFP-BGHpA and AAV2/1-SYN-GFP-BGHpA (Fig $2A_1$–$2C_1$). We randomly selected approximately 300 GFP-expressing cells around the injection sites, and examined the neuronal specificity with NeuN immunoreactivity (Fig $2A_2$–$2C_4$). Almost all GFP-expressing cells showed immunoreactivity for NeuN in the CPu with AAV2/1-SynTetOff-GFP and AAV2/1-SYN-GFP-BGHpA (99.4% ± 1.0% and 100% ± 0.0%, respectively, mean ± SD; Fig 2D), indicating that these vectors work specifically in neuronal cells. On the other hand, a significant number of GFP-expressing cells were negative for NeuN immunoreactivity with AAV2/1-CMV-GFP-BGHpA (75.5% ± 5.5%; Fig 2D), since the CMV promoter is a ubiquitous promoter.

We then randomly selected more than 100 GFP-expressing neurons from three mice, and analyzed the expression levels by measuring the average intensity of GFP-NF in the cell bodies. The intensity was 43.3- or 34.3-fold stronger with AAV2/1-SynTetOff-GFP than with AAV2/1-CMV-GFP-BGHpA or AAV2/1-SYN-GFP-BGHpA, respectively (Fig 2E). Although the activity of the CMV promoter was significantly higher than that of the SYN promoter in Neuro-2a cells (Fig 1C) and embryonic mouse spinal cord culture with AAV9 vectors [31], we detected no significant difference between these two promoters *in vivo*. The present findings indicate that the AAV-SynTetOff platform is suitable for strong and neuron-specific gene transduction *in vivo*.

Clear visualization of neuronal processes with modified GFP

To visualize axon fibers efficiently, we modified GFP by adding the following plasma membrane-targeting signals: a palmitoylation signal (palGFP) [32, 35–39] or a myristoylation/

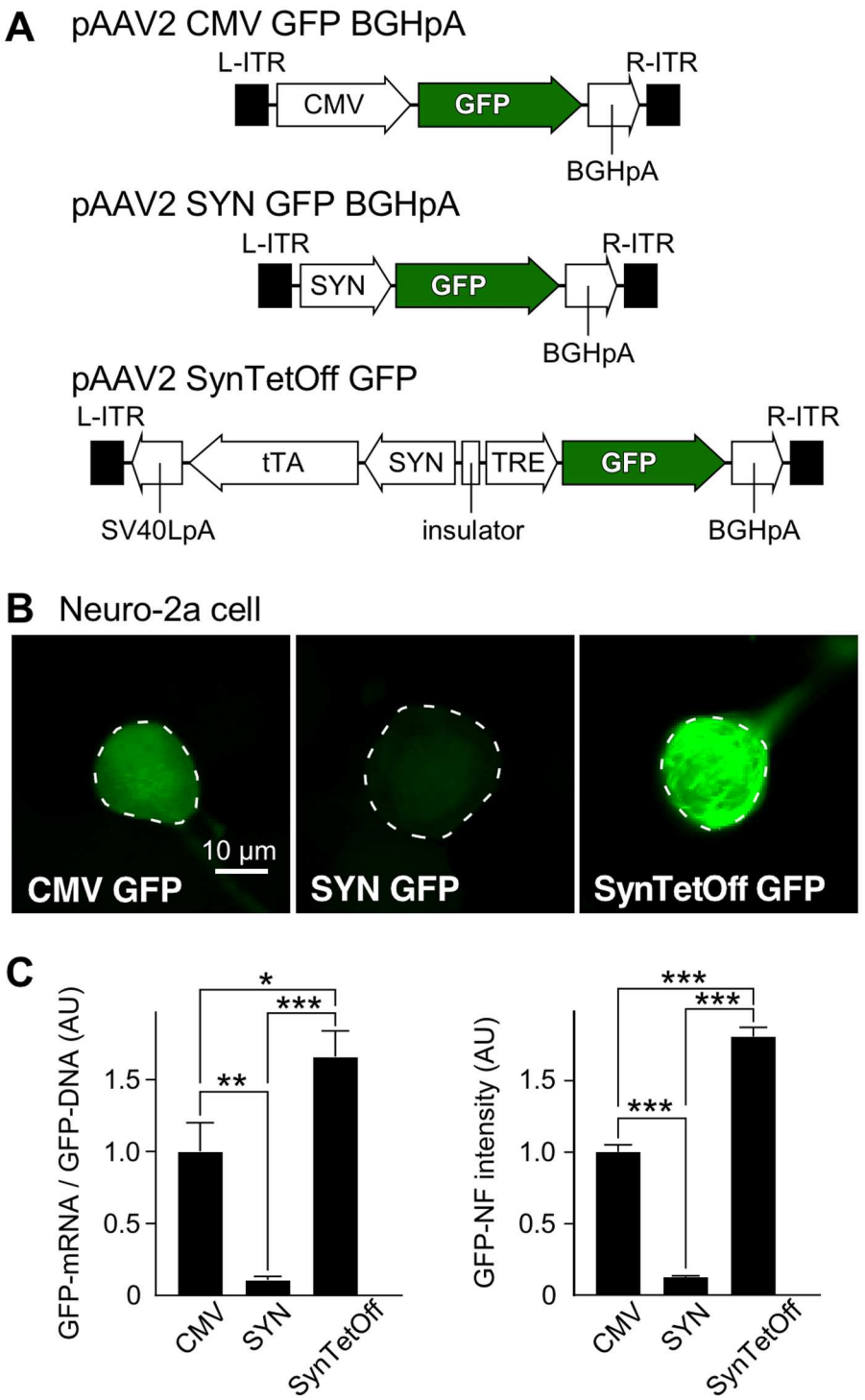

Fig 1. Efficient gene-transduction with AAV-SynTetOff vector *in vitro*. (**A**) Construction of the vector plasmids, pAAV2-CMV-GFP-BGHpA, pAAV2-SYN-GFP-BGHpA, and pAAV2-SynTetOff-GFP. (**B**) One week after infection of Neuro-2a cells with AAV2/1-CMV-GFP-BGHpA, AAV2/1-SYN-GFP-BGHpA, and AAV2/1-SynTetOff-GFP, GFP-NF intensities were measured in the infected cells (outlined by dotted lines with ImageJ). (**C**) The gene-transduction efficiency with AAV2/1-CMV-GFP-BGHpA, AAV2/1-SYN-GFP-BGHpA, or AAV2/1-SynTetOff-GFP was examined quantitatively. The GFP-mRNA/GFP-DNA ratio and the GFP-NF intensity of cells infected with AAV2/1-CMV-GFP-BGHpA were standardized as 1 arbitrary unit (AU). A qRT-PCR assay revealed that GFP-mRNA expression was 1.7- and 15.6-fold higher with AAV2/1-SynTetOff-

GFP than with AAV2/1-CMV-GFP-BGHpA and AAV2/1-SYN-GFP-BGHpA, respectively (normalized to GFP-DNA levels). GFP-NF intensities showed similar ratios to AAV2/1-CMV-GFP-BGHpA and AAV2/1-SYN-GFP-BGHpA (factors of 1.8 and 14.4, respectively), indicating that the GFP-NF intensities reflected GFP-mRNA expression levels. Error bars, ± standard error of the mean (SEM). *$p < 0.05$, **$p < 0.01$, ***$p < 0.001$.

doi:10.1371/journal.pone.0169611.g001

palmitoylation signal (myrGFP) [39] (Fig 3A). One week after the injection of AAV2/1-Syn-TetOff-GFP, AAV2/1-SynTetOff-palGFP, and AAV2/1-SynTetOff-myrGFP into the mouse CPu, we observed GFP-NF around the injection sites as well as the projection targets such as the external segment of the globus pallidus (GPe) and the substantia nigra pars reticulata (SNr; Fig 3B$_1$–3D$_3$). Strong GFP-NF was observed around the injection sites with these AAV vectors. GFP-NF with AAV2/1-SynTetOff-GFP was weak in the GPe and very weak in the SNr (Fig 3B$_4$ and 3B$_5$). On the other hand, the axon fibers of neostriatal neurons, which are presumably medium-sized spiny neurons, were clearly visualized with membrane-targeted GFP, especially with palGFP (Fig 3C$_4$–3D$_5$). These results indicate that the membrane-targeted GFP can be effectively used for visualizing axonal processes.

We then attached the somatodendrite-targeting signal, LDLRct, to the C-terminus of myrGFP (FGL; Fig 3A) [39, 40]. Although intense GFP-NF was observed around the injection

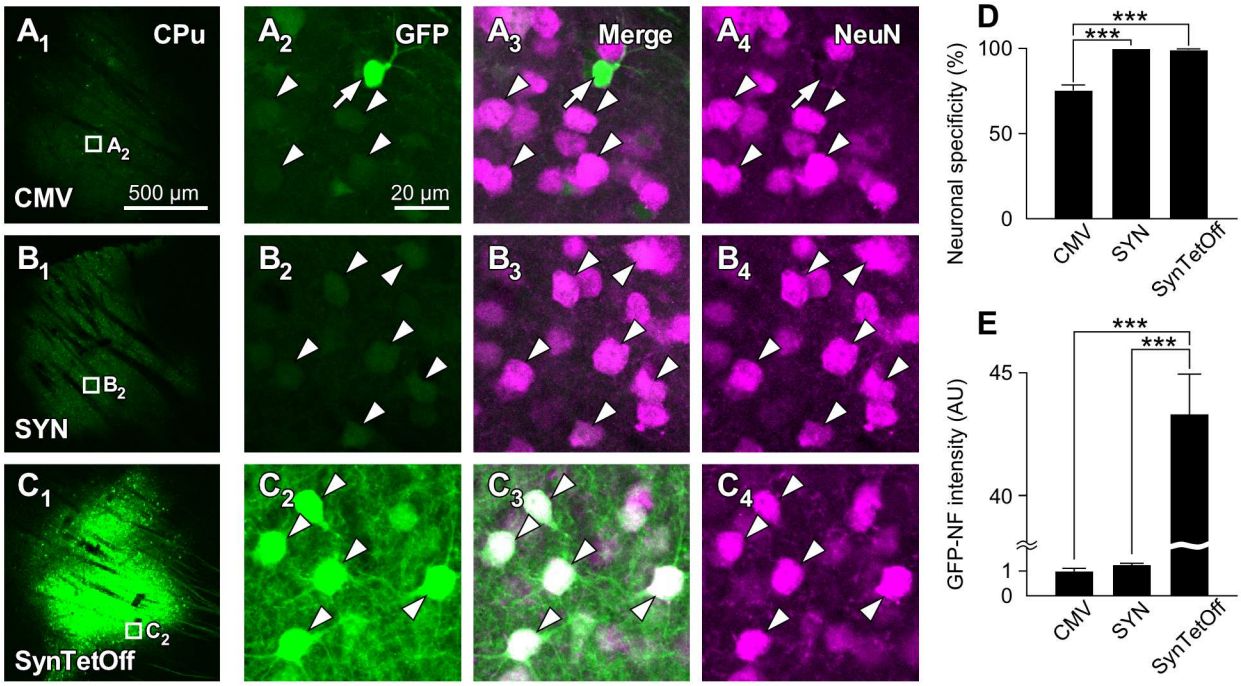

Fig 2. Neuron-specific and high-level transgene expression with the AAV-SynTetOff-GFP vector *in vivo*. (**A$_1$–C$_4$**) One week after the injection of the AAV vectors, GFP-NF was observed in the caudate-putamen (CPu). Cells infected with the vector AAV2/1-SynTetOff-GFP (C) were more strongly labeled with GFP than those infected with the vectors AAV2/1-CMV-GFP-BGHpA (A) and AAV2/1-SYN-GFP-BGHpA (B). Almost all GFP-positive cells were also immunoreactive for NeuN with AAV2/1-SYN-GFP-BGHpA (B$_2$–B$_4$, arrowheads) and AAV2/1-SynTetOff-GFP (C$_2$–C$_4$, arrowheads), whereas some GFP-positive cells were negative for NeuN with the AAV2/1-CMV-GFP-BGHpA vector (A$_2$–A$_4$, arrow; a putative glial cell). Scale bar in A$_1$ applies to A$_1$–C$_1$; Scale bar in A$_2$ applies to A$_2$–A$_4$, B$_2$–B$_4$, and C$_2$–C$_4$. (**D**) Specificities of GFP expression in neostriatal neurons. AAV2/1-SYN-GFP-BGHpA and AAV2/1-SynTetOff-GFP displayed specific expression in neuronal cells, while the expression of GFP with AAV2/1-CMV-GFP-BGHpA was not neuron-specific. (**E**) GFP-NF intensities in neostriatal neurons. The mean GFP-NF intensity with AAV2/1-CMV-GFP-BGHpA was standardized as 1 AU. AAV2/1-SynTetOff-GFP transduced much stronger GFP expression in neurons than AAV2/1-CMV-GFP-BGHpA and AAV2/1-SYN-GFP-BGHpA (factors of 43.3 and 34.3, respectively). Error bars, ± SEM. *$p < 0.05$, **$p < 0.01$, ***$p < 0.001$.

doi:10.1371/journal.pone.0169611.g002

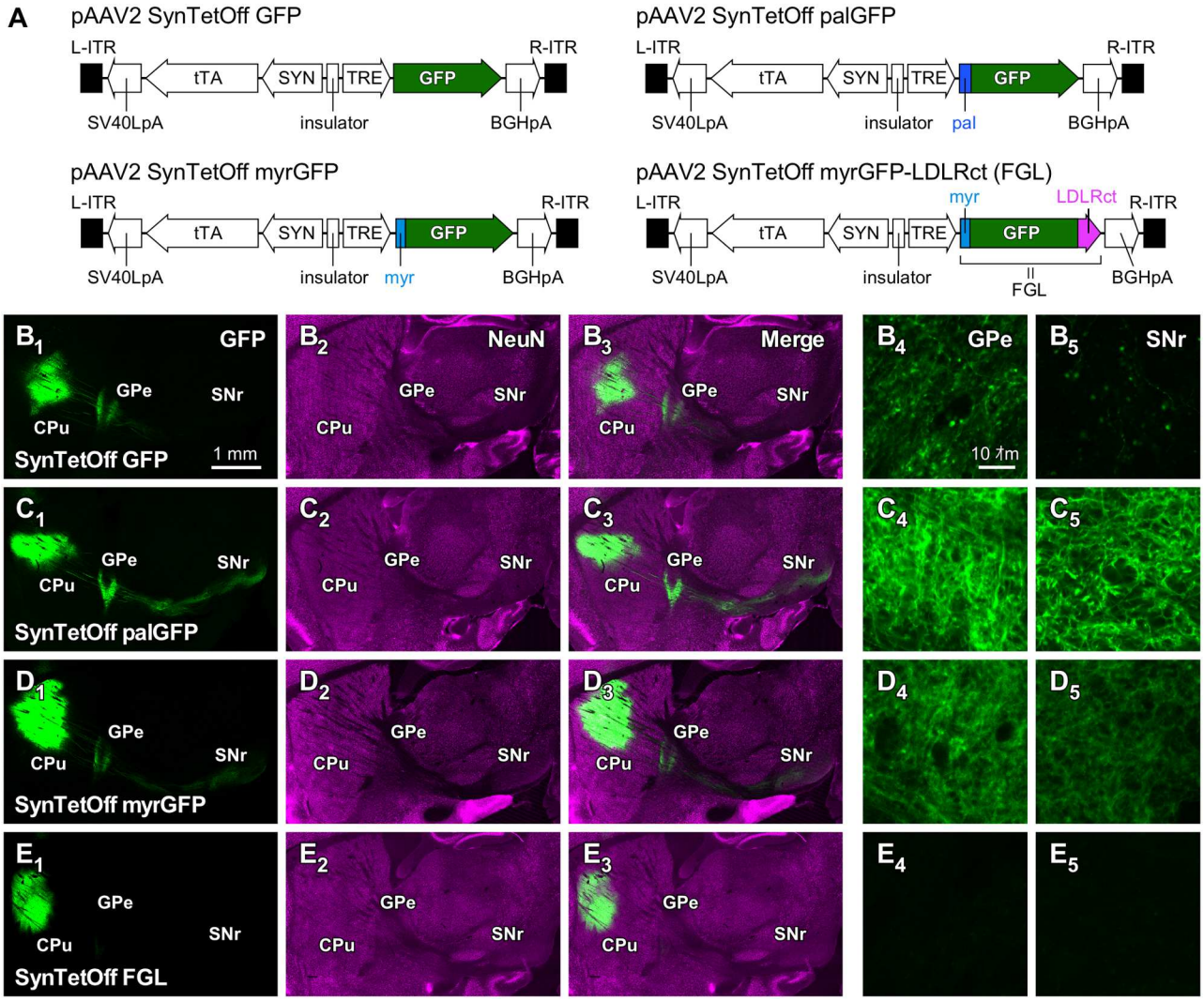

Fig 3. Axon labeling of neostriatal neurons with the AAV-SynTetOff vectors. (**A**) Construction of the vector plasmids, pAAV2-SynTetOff-GFP, pAAV2-SynTetOff-palGFP, pAAV2-SynTetOff-myrGFP, and pAAV2-SynTetOff-FGL. (**B–E**) Sagittal views of brain sections with injections of the AAV vectors. By addition of the palmitoylation site of the GAP-43 N-terminus (palGFP; C) or the myristoylation/palmitoylation site of the Fyn N-terminus (myrGFP; D), axon fibers in the GPe and SNr were more clearly visualized than with GFP without membrane-targeting signal (B). On the other hand, when a somatodendritic-targeting signal, LDLRct, was added to the C-terminus of myrGFP (FGL; E), axon fiber labeling in the GPe and SNr was mostly suppressed (E_4, E_5). Scale bar in B_1 applies to B_1–E_1, B_2–E_2, and B_3–E_3. Scale bar in B_4 applies to B_4–E_4 and B_5–E_5.

doi:10.1371/journal.pone.0169611.g003

sites, almost no signal was found in the GPe and SNr (Fig $3E_1$–$3E_5$). As reported in a previous study with a lentivirus vector [39], the somatodendritic membrane-targeted GFP efficiently labeled the somatodendritic domains of the infected neurons, but not the axonal structures, with AAV-SynTetOff-FGL.

To demonstrate the effects of the membrane- and/or dendrite-targeting signals, we generated an AAV vector that expressed both FGL and palmRFP1 (Fig 4A). One week after injection of this vector, we observed the distribution of GFP-NF and mRFP1-NF. As expected, GFP-NF was restricted within the CPu, whereas mRFP1-NF was clearly observed not only in the CPu but also in the GPe and SNr (Fig $4B_1$–$4B_3$). We further performed immunofluorescence staining for MAP2, which is considered a marker for dendrites (Fig $4C_1$–$4D_4$). Dendrites labeled

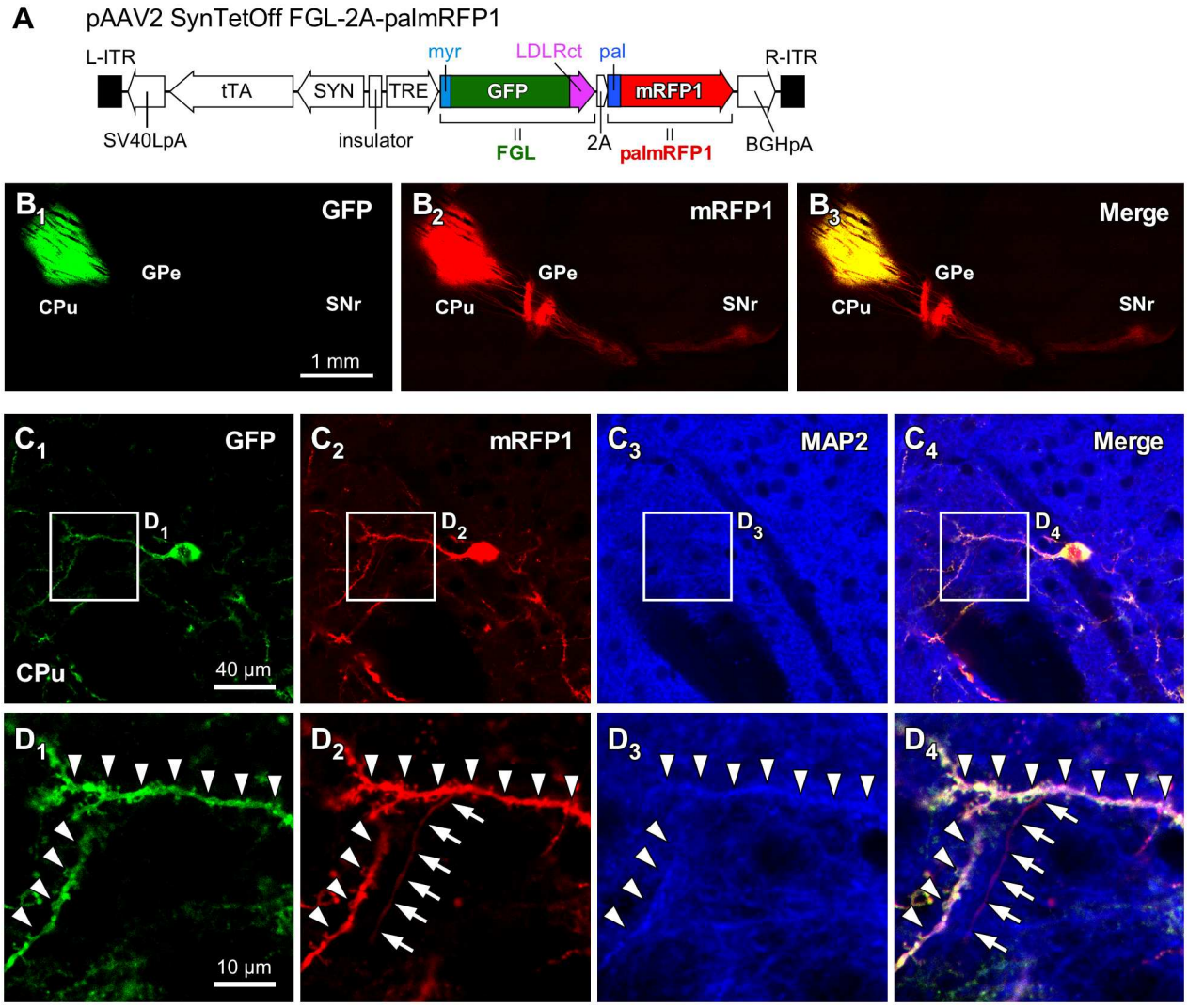

Fig 4. Dual-color labeling of the somatodendritic and axonal structures of neostriatal neurons with the AAV-SynTetOff vectors. (**A**) Construction of the vector plasmid, pAAV2-SynTetOff-FGL-2A-palmRFP1. (**B**) Sagittal view of brain sections with injection of AAV2/1-SynTetOff-FGL-2A-palmRFP1 into the CPu. This AAV vector expressed both FGL and palmRFP1 in the infected neurons. GFP-NF was restricted to the CPu, and mRFP1-NF was observed not only in the CPu but also the GPe and SNr, where neostriatal neurons project. (**C**) After immunofluorescence staining for MAP2 (blue), the sections were observed under a confocal laser scanning microscope in the CPu. (**D**) High-magnification images in (C). Arrowheads and arrows indicate the dendritic and axonal structures, respectively. Scale bar in B_1 applies to B_1–B_3. Scale bar in C_1 applies to C_2–C_4. Scale bar in D_1 applies to D_2–E_4.

doi:10.1371/journal.pone.0169611.g004

with both GFP and mRFP1 displayed immunoreactivity for MAP2 (Arrowheads in Fig 4D). On the other hand, the axon fiber was visualized with mRFP1 but not GFP, and was negative for MAP2 immunoreactivity (Arrows in Fig 4D). These results clearly show that the somatodendritic-targeting signal effectively localizes GFP and that the axons can be distinguished by the presence of mRFP1 signal and the absence of GFP signal.

This vector, AAV2/1-SynTetOff-FGL-2A-palmRFP1, might be useful for elucidating the differential distributions of somatodendritic and axonal structures without reconstruction of the infected neurons. In the subsequent experiment, we applied this vector to one of the neocortical GABAergic neurons, to demonstrate the usefulness of the dual-color labeling.

Differential distributions of dendrites and axons of VIP+ neurons

VIP+ neurons are one of the subclasses of GABAergic neurons in the neocortex, and are mainly distributed in layer (L) L2/3 [54–56]. Most VIP+ neurons in the neocortex bidirectionally extend their dendrites in the vertical orientation, and the axon fibers run vertically and translaminarly across cortical layers. On the basis of the characteristic features of the dendrites and axons, VIP+ neurons in the neocortex have been classified as bipolar/modified bipolar/bitufted cells and double bouquet cells [57–60].

Contrary to the vertical arborizations, the somatodendritic and axonal distributions of VIP+ neurons in the tangential/horizontal direction are yet to be clarified. In a previous immunohistochemical study, VIP immunoreactivity was unevenly observed in L4 of the rodent S1BF [61, 62]. There are "barrels" and inter-barrel "septa" in L4 of the S1BF, and each barrel-related column in the rodent S1BF receives input from the corresponding vibrissa of the contralateral whisker pad [63–67]. While the immunoreactivity for vesicular glutamate transporter 2 (VGluT2), which is a marker for thalamocortical axon terminals [68–70], is higher in barrels than in septa [71–73], the immunoreactivity for VIP is higher in septa than in barrels [61, 62]. By applying the dual-color labeling method described above, we analyzed the somatodendritic and axonal distributions of L2/3 VIP+ neurons in the S1BF to identify whether the higher immunoreactivity for VIP in septa is derived from dendrites or axons.

One week after the injection of AAV2/1-SynTetOff-FLEX-FGL-2A-palmRFP1 into the superficial layer in the S1BF of VIP-Cre knock-in mice, we observed the immunoreactivities for GFP and mRFP1 under a confocal laser scanning microscope, and selected three samples in which the infection was restricted to L2/3 VIP+ neurons (Fig 5A–5E). The Somata and dendrites of L2/3 VIP+ neurons were labeled with GFP, whereas their axons as well as somatodendrites were visualized with mRFP1 (Fig 5B and 5C). After binarization of the images of immunofluorescence-stained sections for GFP and mRFP1 (Fig 5F and 5G), the binary image of GFP was subtracted from that of mRFP1 (Fig 5H). The binarized signals of GFP represented the somatodendritic distribution of L2/3 VIP+ neurons (Fig 5F), whereas the subtracted image represented their axonal distribution (Fig 5H).

The somatodendritic and axonal distributions were first quantified vertically from the pia mater to the white matter (Fig 5I). The distribution of the dendrites of L2/3 VIP+ neurons was largely restricted to the regions between L1 and L4, whereas the axons were present from L1 to L6, consistent with previous studies [57–59]. Given the vertical arborization of L2/3 VIP+ neuron axon fibers within a small tangential expansion [74], their outputs diverge to the deep layer within the vertical modules (e.g. a columnar structure), though they receive synaptic inputs in the upper layer.

We subsequently examined the dendritic and axonal distributions of L2/3 VIP+ neurons in the tangential direction (Fig 5J–5N). In L4, the distribution of dendrites was not different between barrels and septa, whereas axons obviously preferred septa to barrels (Fig 4M). On the other hand, axonal distribution in other layers was not different between barrel- and septa-related columns (Fig 5N). These results indicate that L2/3 VIP+ neurons send axons to L1–6, with preferential placement in L4 through septa.

Discussion

High-level gene transduction with the AAV-SynTetOff vector

AAV vectors are one of the most useful gene-transfer systems, and a variety of AAV vectors have been developed with ubiquitous or neuron-specific promoters, including the CMV or SYN promoters, to improve the expression levels and/or cell-type specificities [75–78]. In the

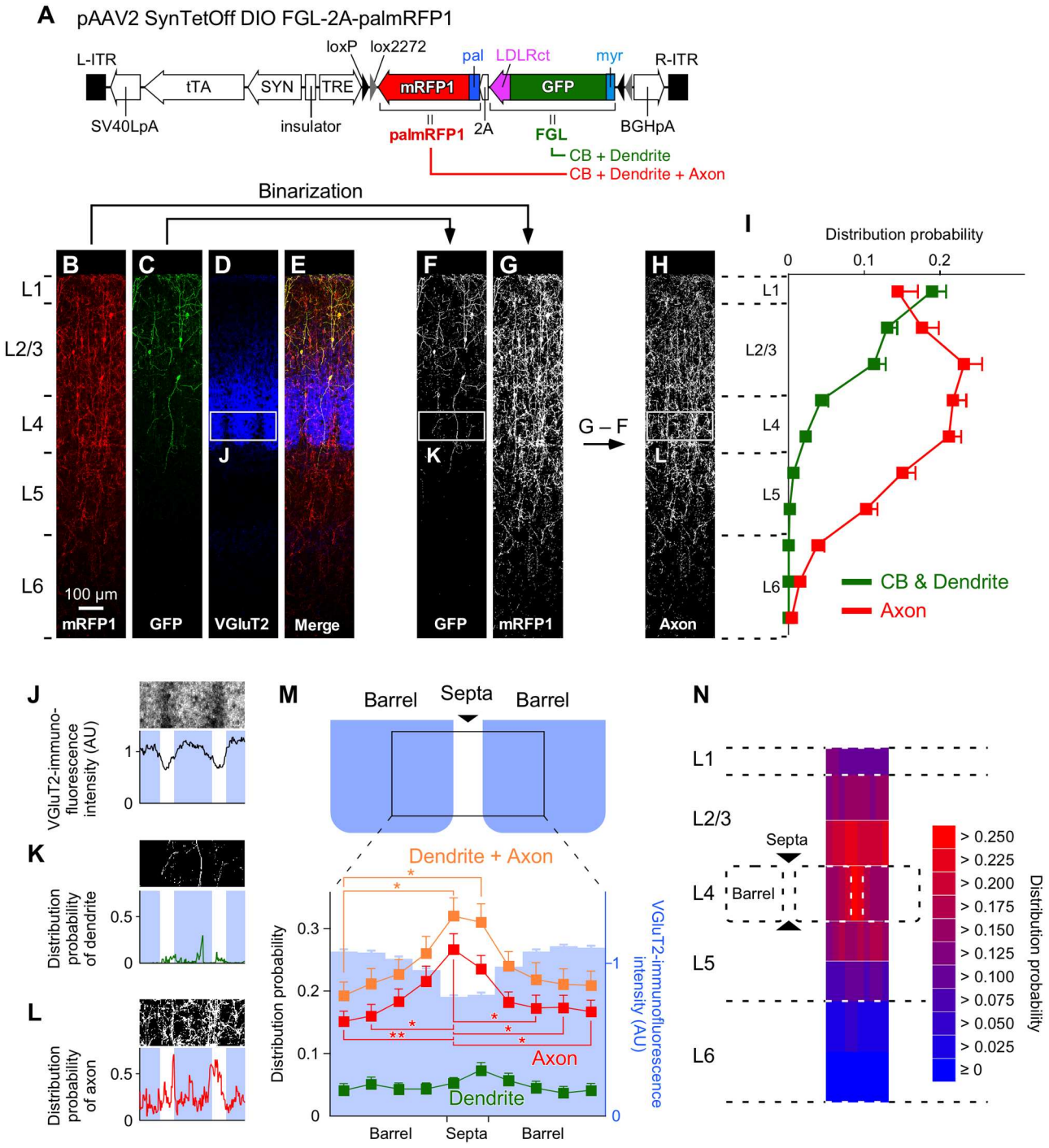

Fig 5. Differential distributions of the dendrites and axons of L2/3 VIP+ neurons in the S1BF. (**A**) Construction of the vector plasmid, pAAV2-SynTetOff-FLEX-FGL-2A-palmRFP1. (**B–E**) Coronal sections immunostained for mRFP1 (B), GFP (C), and VGluT2 (D). Scale bar in B applies to B–E. (**F**, **G**) Binarization of the images for GFP and mRFP1. The binary image of GFP signals (F) represents the somatodendritic distribution of L2/3 VIP+ neurons. (**H**) Axonal distribution was estimated by subtracting the binarized image for GFP (F) from that for mRFP1 (G). (**I**) The distribution probabilities of the somatodendrites and axons of L2/3 VIP+ neurons across cortical layers. (**J**) VGluT2-immunofluorescence intensity in the tangential direction in L4 of the S1BF. Blue indicates barrel locations. (**K**, **L**) The distribution probabilities of the dendrites (K) or axons (L) of L2/3 VIP+ neurons in L4 of the S1BF. (**M**) Mean distribution probabilities of the dendrites and/or axons of L2/3 VIP+ neurons in L4 of the S1BF. The probabilities are plotted between the centers of adjacent barrels. The tangential width was divided into 10 bins. Blue bars represent VGluT2 immunofluorescence intensities. (**N**) Axonal distributions of L2/3 VIP+ neurons in the S1BF. The vertical widths of L2/3, L5, and L6 were divided by a factor of 2 at the center of each layer. The distribution probability of the

axons in L4 was higher in septa than in barrels, whereas those in the other layers were not significantly different between the barrel- and septa-related columns. Error bars, ± SEM. *$p < 0.05$, **$p < 0.01$.

doi:10.1371/journal.pone.0169611.g005

present study, we incorporated a neuron-specific promoter (SYN promoter) and the Tet-Off system into a single vector, and successfully achieved both neuronal specificity and strong gene transduction. The SYN promoter expressed tTAad specifically in neuronal cells, and then, the TRE promoter induced strong transduction of the reporter protein. The Tet-Off system is known to amplify transcriptional activities [32, 79, 80]. The AAV-SynTetOff vector might be suitable for the efficient labeling of neuronal cells, since the vector can produce large amounts of protein in the infected cells. In addition, replacing the SYN promoter sequence with the desired sequence will enable the induction of high-level expression of transgene(s) in other type(s) of cells.

We assessed the gene-transduction efficiency of the AAV-SynTetOff vector by calculating the ratio of GFP-mRNA/GFP-DNA and GFP-NF intensity in Neuro-2a cells, and demonstrated that the ratio was comparable to that of GFP-NF intensity; the ratio with the AAV-SynTetOff vector was 1.7- and 15.6-fold higher than that with the CMV and SYN promoters, respectively, and GFP-NF intensity with the AAV-SynTetOff vector was 1.8- and 14.4-times higher than that with the CMV and SYN promoters, respectively. Since the GFP-mRNA/GFP-DNA ratio and GFP-NF intensity are assumed to reflect the transcriptional activity and protein expression level, the gene-transduction efficiency can be estimated by measuring GFP-NF intensity in the infected cells. However, the *in vitro* and *in vivo* gene-transduction efficiencies estimated by using GFP-NF were different. While the GFP-NF intensity in the neostriatal neurons infected with AAV-SynTetOff was 43.3-fold higher than that observed with the conventional AAV vector containing the CMV promoter, the difference in GFP-NF intensity in Neuro-2a cells between the two vectors was only 1.8-fold. This discrepancy might be attributable to the differences in cell types between neostriatal neurons and Neuro-2a cells. The gene-transduction efficiency of the AAV-SynTetOff vector may be different in various cell types, and this needs to be confirmed in every experiment.

In our previous studies, we developed lentivirus vectors equipped with the Tet-Off system [32, 33], and achieved high-level gene transduction compared with conventional lentivirus vectors. However, it was technically difficult to prepare lentivirus vectors that carried both tTAad and the TRE promoter within a single backbone in high titer [32, 33]. The preparation of AAV vectors in high titer is easier than preparing lentivirus vectors [81]. In addition, AAV vectors are more efficient in gene transfer to central neurons than lentivirus vectors pseudotyped with the VSV glycoprotein (VSV-G) [81]. Therefore, the AAV-SynTetOff vectors may be more promising than the single Tet-Off lentivirus vectors for transgene delivery to central neurons.

Dual fluorescence labeling with single AAV-SynTetOff vectors

Neostriatal projection neurons, which account for 90%–95% of all neostriatal neurons, comprise both direct and indirect pathway neurons [82]; direct pathway neurons directly project to the output nuclei, the internal segment of the globus pallidus (GPi) and SNr, though some of them send axon collaterals to the GPe [83], while the indirect pathway neurons send axons exclusively to the GPe. In the present study, we injected virus vectors into the CPu to evaluate the efficiency of axonal labeling in the projection neurons.

The AAV-SynTetOff vectors expressing membrane-targeting signal-attached GFP (palGFP or myrGFP) visualized the axon fibers of neostriatal projection neurons more efficiently than the vector without the membrane-targeting signal (Fig 3B–3D). On the other hand, as reported

previously [39], the dendrite-targeting signal, LDLRct, strongly suppressed the axonal labeling of neostriatal projection neurons infected by AAV2/1-SynTetOff-FGL (Fig 3E). In the present study, we generated the vector AAV2/1-SynTetOff-FGL-2A-palmRFP1, which expresses both FGL and palmRFP1, to visualize the somatodendritic and axonal structures in different colors (Fig 3F). After injection of the vector into the CPu, the axons of neostriatal projection neurons were labeled only by palmRFP1, whereas the somatodendritic structures were visualized by FGL and palmRFP1 (Fig 3G). Thus, this vector might be useful to distinguish the somatodendritic and axonal arborizations of the infected neurons by observing fluorescent signals.

We then applied this dual fluorescence labeling method to VIP+ neurons in the neocortex, which account for only a small fraction of neocortical GABAergic neurons [54, 55, 84–87], to analyze the somatodendritic and axonal distribution of L2/3 VIP+ neurons at the population level. After injection of AAV2/1-SynTetOff-FLEX-FGL-2A-palmRFP1 into the S1BF of VIP-Cre knock-in mice, the somatodendritic structures of L2/3 VIP+ neurons were labeled with FGL, whereas the whole structure, including the axons, were visualized by palmRFP1 (Fig 5B and 5C). After binarization of the images, the somatodendritic and axonal distributions were quantitatively analyzed through the cortical depth (Fig 5F–5I). To date, to quantitatively analyze the somatodendritic and axonal distributions, it is necessary to trace and reconstruct the dense dendritic and axonal ramifications of each neuron, and the reconstruction of many single neurons is laborious and impractical. The present method, which involves dual fluorescence labeling by the AAV vector, would be valuable to clarify the information flow from dendrites to axons at the population level without tracing and reconstruction of a particular subset of neurons.

Somatodendritic and axonal arborizations of L2/3 VIP+ neurons in the S1BF

VIP+ neurons are now attracting a great deal of attention in the study of the neocortical circuit. VIP+ neurons in the neocortex potentiate pyramidal cell excitability by inhibiting other types of inhibitory neurons [88–92]. Through this "disinhibitory circuit," VIP+ neurons are assumed to translaminarly trigger cortical activation within a columnar or subcolumnar structure to facilitate local cortical processing and sensory responses.

The immunoreactivity for VIP is higher in septa than in barrels of the S1BF [61, 62]. Since immunostaining for VIP labels the somata, dendrites and axons of VIP+ neurons, it has not yet been determined which structures, the somatodendrites or axons of VIP+ neurons, prefer septa to barrels. To address this question, we injected the vector AAV2/1-SynTetOff-FLEX-FGL-2A-palmRFP1 into the S1BF of VIP-Cre knock-in mice, and analyzed the somatodendritic and axonal domains of L2/3 VIP+ neurons.

Vertical dendritic expansion was largely restricted to the regions between L1 and L4, whereas axons were present from L1 to L6 (Fig 5I), consistent with a previous study [59]. We then identified septa-preferential axonal arborization of L2/3 VIP+ neurons. Their dendritic arborization showed no significant difference between barrels and septa, indicating that L2/3 VIP+ neurons receive inputs from L4 without distinction between barrels and septa. On the other hand, L2/3 VIP+ neurons sent axon fibers significantly more densely to septa than to barrels.

The thalamocortical projection from the anterior subdivision of the posteromedial nucleus and the corticocortical projections originating from other cortical areas such as the primary motor cortex specifically target septa [93–95]. These paralemniscal projections and interareal connections are considered crucial for the context-dependent sensory processing of pyramidal cells evoked by tactile stimulation and sensorimotor integration [96–98]. Therefore, the septa-

preferential output of L2/3 VIP+ neurons might affect these integrative inputs in septa of the S1BF.

Future direction

In the present study, we demonstrated high-level expression of transgenes with the AAV-SynTetOff vectors and efficient labeling of central neurons. Furthermore, by attaching the membrane-targeting and/or dendrite-targeting signals, the somatodendritic and/or axonal structures of the infected neurons were clearly visualized. Recently, many kinds of tissue-clearing methods have been developed, such as Scale [99, 100], CUBIC [101, 102], CLARITY [103, 104], SeeDB [105, 106], DISCO [107–109], etc. Although these techniques enable us to perform three-dimensional imaging with whole brain or thick-slice samples in large-scale, the intensity of fluorescent signal is critical for deep brain imaging and comprehensive analysis of neuronal structures [99]. The AAV-SynTetOff vectors, which achieve high-level expression of reporter protein(s), would prompt the morphological analysis of neuronal circuits and large-scale connectomic mapping with these tissue-clearing methods.

Supporting Information

S1 Table. Primers and oligonucleotides used in the present study.
(DOCX)

Acknowledgments

The authors thank Prof. Takeshi Kaneko for his helpful suggestions.

Author Contributions

Conceptualization: JS TF HH.

Data curation: JS HH.

Formal analysis: JS HH.

Funding acquisition: JS TF HH.

Investigation: JS MT SO YI HH.

Methodology: JS HH.

Project administration: HH.

Resources: HH.

Supervision: HH.

Visualization: JS HH.

Writing – original draft: JS HH.

Writing – review & editing: JS TF HH.

References

1. Lichtman JW, Sanes JR. Ome sweet ome: what can the genome tell us about the connectome? Curr Opin Neurobiol. 2008; 18(3):346–53. Epub 2008/09/20. doi: 10.1016/j.conb.2008.08.010 PMID: 18801435

2. Bohland JW, Wu C, Barbas H, Bokil H, Bota M, Breiter HC, et al. A proposal for a coordinated effort for the determination of brainwide neuroanatomical connectivity in model organisms at a mesoscopic scale. PLoS Comput Biol. 2009; 5(3):e1000334. Epub 2009/03/28. doi: 10.1371/journal.pcbi.1000334 PMID: 19325892
3. Budd JM, Kisvarday ZF. Communication and wiring in the cortical connectome. Front Neuroanat. 2012; 6:42. Epub 2012/10/23. doi: 10.3389/fnana.2012.00042 PMID: 23087619
4. Kaneko T. Local connections of excitatory neurons in motor-associated cortical areas of the rat. Front Neural Circuits. 2013; 7:75. Epub 2013/06/12. doi: 10.3389/fncir.2013.00075 PMID: 23754982
5. Rockland KS. About connections. Front Neuroanat. 2015; 9:61. Epub 2015/06/05. doi: 10.3389/fnana.2015.00061 PMID: 26042001
6. Jones EG. Neuroanatomy: Cajal and after Cajal. Brain Res Rev. 2007; 55(2):248–55. doi: 10.1016/j.brainresrev.2007.06.001 PMID: 17659350
7. Golgi C. Sulla struttura della sostanza grigia del cervelo. Gazzetta Medica Italiana. Lombardia. 1873; 33:244–46.
8. Gerfen CR, Sawchenko PE. An anterograde neuroanatomical tracing method that shows the detailed morphology of neurons, their axons and terminals: immunohistochemical localization of an axonally transported plant lectin, Phaseolus vulgaris leucoagglutinin (PHA-L). Brain Res. 1984; 290(2):219–38. Epub 1984/01/09. PMID: 6198041
9. Izzo PN. A note on the use of biocytin in anterograde tracing studies in the central nervous system: application at both light and electron microscopic level. J Neurosci Methods. 1991; 36(2–3):155–66. Epub 1991/02/01. PMID: 1712060
10. Kristensson K, Olsson Y. Retrograde axonal transport of protein. Brain Res. 1971; 29(2):363–5. Epub 1971/06/18. PMID: 4107258
11. Stoeckel K, Schwab M, Thoenen H. Role of gangliosides in the uptake and retrograde axonal transport of cholera and tetanus toxin as compared to nerve growth factor and wheat germ agglutinin. Brain Res. 1977; 132(2):273–85. Epub 1977/08/26. PMID: 70259
12. Kobbert C, Apps R, Bechmann I, Lanciego JL, Mey J, Thanos S. Current concepts in neuroanatomical tracing. Prog Neurobiol. 2000; 62(4):327–51. Epub 2000/06/17. PMID: 10856608
13. Lanciego JL, Wouterlood FG. A half century of experimental neuroanatomical tracing. J Chem Neuroanat. 2011; 42(3):157–83. Epub 2011/07/26. doi: 10.1016/j.jchemneu.2011.07.001 PMID: 21782932
14. Vercelli A, Repici M, Garbossa D, Grimaldi A. Recent techniques for tracing pathways in the central nervous system of developing and adult mammals. Brain Res Bull. 2000; 51(1):11–28. Epub 2000/02/02. PMID: 10654576
15. Smith SJ. Circuit reconstruction tools today. Curr Opin Neurobiol. 2007; 17(5):601–8. Epub 2007/12/18. doi: 10.1016/j.conb.2007.11.004 PMID: 18082394
16. Luo L, Callaway EM, Svoboda K. Genetic dissection of neural circuits. Neuron. 2008; 57(5):634–60. Epub 2008/03/18. doi: 10.1016/j.neuron.2008.01.002 PMID: 18341986
17. Feng G, Mellor RH, Bernstein M, Keller-Peck C, Nguyen QT, Wallace M, et al. Imaging neuronal subsets in transgenic mice expressing multiple spectral variants of GFP. Neuron. 2000; 28(1):41–51. Epub 2000/11/22. PMID: 11086982
18. Livet J, Weissman TA, Kang H, Draft RW, Lu J, Bennis RA, et al. Transgenic strategies for combinatorial expression of fluorescent proteins in the nervous system. Nature. 2007; 450(7166):56–62. Epub 2007/11/02. doi: 10.1038/nature06293 PMID: 17972876
19. Tabata H, Nakajima K. Efficient in utero gene transfer system to the developing mouse brain using electroporation: visualization of neuronal migration in the developing cortex. Neuroscience. 2001; 103(4):865–72. Epub 2001/04/13. PMID: 11301197
20. Mizuno H, Luo W, Tarusawa E, Saito YM, Sato T, Yoshimura Y, et al. NMDAR-regulated dynamics of layer 4 neuronal dendrites during thalamocortical reorganization in neonates. Neuron. 2014; 82(2):365–79. doi: 10.1016/j.neuron.2014.02.026 PMID: 24685175
21. Mikuni T, Nishiyama J, Sun Y, Kamasawa N, Yasuda R. High-Throughput, High-Resolution Mapping of Protein Localization in Mammalian Brain by In Vivo Genome Editing. Cell. 2016; 165(7):1803–17. doi: 10.1016/j.cell.2016.04.044 PMID: 27180908
22. Davidson BL, Breakefield XO. Viral vectors for gene delivery to the nervous system. Nat Rev Neurosci. 2003; 4(5):353–64. doi: 10.1038/nrn1104 PMID: 12728263
23. Callaway EM. A molecular and genetic arsenal for systems neuroscience. Trends Neurosci. 2005; 28(4):196–201. doi: 10.1016/j.tins.2005.01.007 PMID: 15808354

24. Taniguchi H, He M, Wu P, Kim S, Paik R, Sugino K, et al. A resource of Cre driver lines for genetic targeting of GABAergic neurons in cerebral cortex. Neuron. 2011; 71(6):995–1013. Epub 2011/09/29. doi: 10.1016/j.neuron.2011.07.026 PMID: 21943598

25. Gerfen CR, Paletzki R, Heintz N. GENSAT BAC cre-recombinase driver lines to study the functional organization of cerebral cortical and basal ganglia circuits. Neuron. 2013; 80(6):1368–83. Epub 2013/12/24. doi: 10.1016/j.neuron.2013.10.016 PMID: 24360541

26. Muzyczka N. Use of adeno-associated virus as a general transduction vector for mammalian cells. Curr Top Microbiol Immunol. 1992; 158:97–129. Epub 1992/01/01. PMID: 1316261

27. Xiao X, Li J, McCown TJ, Samulski RJ. Gene transfer by adeno-associated virus vectors into the central nervous system. Exp Neurol. 1997; 144(1):113–24. Epub 1997/03/01. doi: 10.1006/exnr.1996.6396 PMID: 9126160

28. Peel AL, Klein RL. Adeno-associated virus vectors: activity and applications in the CNS. J Neurosci Methods. 2000; 98(2):95–104. Epub 2000/07/06. PMID: 10880823

29. Gholizadeh S, Tharmalingam S, Macaldaz ME, Hampson DR. Transduction of the central nervous system after intracerebroventricular injection of adeno-associated viral vectors in neonatal and juvenile mice. Hum Gene Ther Methods. 2013; 24(4):205–13. doi: 10.1089/hgtb.2013.076 PMID: 23808551

30. Gray SJ, Foti SB, Schwartz JW, Bachaboina L, Taylor-Blake B, Coleman J, et al. Optimizing promoters for recombinant adeno-associated virus-mediated gene expression in the peripheral and central nervous system using self-complementary vectors. Hum Gene Ther. 2011; 22(9):1143–53. doi: 10.1089/hum.2010.245 PMID: 21476867

31. Lukashchuk V, Lewis KE, Coldicott I, Grierson AJ, Azzouz M. AAV9-mediated central nervous system-targeted gene delivery via cisterna magna route in mice. Mol Ther Methods Clin Dev. 2016; 3:15055. doi: 10.1038/mtm.2015.55 PMID: 26942208

32. Hioki H, Kuramoto E, Konno M, Kameda H, Takahashi Y, Nakano T, et al. High-level transgene expression in neurons by lentivirus with Tet-Off system. Neurosci Res. 2009; 63(2):149–54. Epub 2008/11/26. doi: 10.1016/j.neures.2008.10.010 PMID: 19028532

33. Watakabe A, Kato S, Kobayashi K, Takaji M, Nakagami Y, Sadakane O, et al. Visualization of cortical projection neurons with retrograde TET-off lentiviral vector. PLoS One. 2012; 7(10):e46157. Epub 2012/10/17. doi: 10.1371/journal.pone.0046157 PMID: 23071541

34. Campbell RE, Tour O, Palmer AE, Steinbach PA, Baird GS, Zacharias DA, et al. A monomeric red fluorescent protein. Proc Natl Acad Sci U S A. 2002; 99(12):7877–82. doi: 10.1073/pnas.082243699 PMID: 12060735

35. Moriyoshi K, Richards LJ, Akazawa C, O'Leary DD, Nakanishi S. Labeling neural cells using adenoviral gene transfer of membrane-targeted GFP. Neuron. 1996; 16(2):255–60. PMID: 8789941

36. Okada A, Lansford R, Weimann JM, Fraser SE, McConnell SK. Imaging cells in the developing nervous system with retrovirus expressing modified green fluorescent protein. Exp Neurol. 1999; 156(2):394–406. Epub 1999/05/18. doi: 10.1006/exnr.1999.7033 PMID: 10328944

37. Tamamaki N, Nakamura K, Furuta T, Asamoto K, Kaneko T. Neurons in Golgi-stain-like images revealed by GFP-adenovirus infection in vivo. Neurosci Res. 2000; 38(3):231–6. Epub 2000/11/09. PMID: 11070189

38. Furuta T, Tomioka R, Taki K, Nakamura K, Tamamaki N, Kaneko T. In vivo transduction of central neurons using recombinant Sindbis virus: Golgi-like labeling of dendrites and axons with membrane-targeted fluorescent proteins. J Histochem Cytochem. 2001; 49(12):1497–508. Epub 2001/11/29. PMID: 11724897

39. Kameda H, Furuta T, Matsuda W, Ohira K, Nakamura K, Hioki H, et al. Targeting green fluorescent protein to dendritic membrane in central neurons. Neurosci Res. 2008; 61(1):79–91. Epub 2008/03/18. doi: 10.1016/j.neures.2008.01.014 PMID: 18342383

40. Kameda H, Hioki H, Tanaka YH, Tanaka T, Sohn J, Sonomura T, et al. Parvalbumin-producing cortical interneurons receive inhibitory inputs on proximal portions and cortical excitatory inputs on distal dendrites. Eur J Neurosci. 2012; 35(6):838–54. Epub 2012/03/21. doi: 10.1111/j.1460-9568.2012.08027.x PMID: 22429243

41. Hioki H, Kameda H, Nakamura H, Okunomiya T, Ohira K, Nakamura K, et al. Efficient gene transduction of neurons by lentivirus with enhanced neuron-specific promoters. Gene Ther. 2007; 14(11):872–82. doi: 10.1038/sj.gt.3302924 PMID: 17361216

42. Hermening S, Kugler S, Bahr M, Isenmann S. Improved high-capacity adenoviral vectors for high-level neuron-restricted gene transfer to the CNS. J Virol Methods. 2006; 136(1–2):30–7. doi: 10.1016/j.jviromet.2006.03.031 PMID: 16672163

43. Kugler S, Meyn L, Holzmuller H, Gerhardt E, Isenmann S, Schulz JB, et al. Neuron-specific expression of therapeutic proteins: evaluation of different cellular promoters in recombinant adenoviral vectors. Mol Cell Neurosci. 2001; 17(1):78–96. doi: 10.1006/mcne.2000.0929 PMID: 11161471

44. Kawashima T, Okuno H, Nonaka M, Adachi-Morishima A, Kyo N, Okamura M, et al. Synaptic activity-responsive element in the Arc/Arg3.1 promoter essential for synapse-to-nucleus signaling in activated neurons. Proc Natl Acad Sci U S A. 2009; 106(1):316–21. doi: 10.1073/pnas.0806518106 PMID: 19116276

45. Nishino E, Yamada R, Kuba H, Hioki H, Furuta T, Kaneko T, et al. Sound-intensity-dependent compensation for the small interaural time difference cue for sound source localization. J Neurosci. 2008; 28(28):7153–64. doi: 10.1523/JNEUROSCI.4398-07.2008 PMID: 18614685

46. Shoji M, Yoshizaki S, Mizuguchi H, Okuda K, Shimada M. Immunogenic comparison of chimeric adenovirus 5/35 vector carrying optimized human immunodeficiency virus clade C genes and various promoters. PLoS One. 2012; 7(1):e30302. doi: 10.1371/journal.pone.0030302 PMID: 22276174

47. Schnutgen F, Doerflinger N, Calleja C, Wendling O, Chambon P, Ghyselinck NB. A directional strategy for monitoring Cre-mediated recombination at the cellular level in the mouse. Nat Biotechnol. 2003; 21(5):562–5. doi: 10.1038/nbt811 PMID: 12665802

48. Kataoka N, Hioki H, Kaneko T, Nakamura K. Psychological stress activates a dorsomedial hypothalamus-medullary raphe circuit driving brown adipose tissue thermogenesis and hyperthermia. Cell Metab. 2014; 20(2):346–58. doi: 10.1016/j.cmet.2014.05.018 PMID: 24981837

49. Suzuki Y, Kiyokage E, Sohn J, Hioki H, Toida K. Structural basis for serotonergic regulation of neural circuits in the mouse olfactory bulb. J Comp Neurol. 2015; 523(2):262–80. doi: 10.1002/cne.23680 PMID: 25234191

50. Hamamoto M, Kiyokage E, Sohn J, Hioki H, Harada T, Toida K. Structural Basis for Cholinergic Regulation of Neural Circuits in the Mouse Olfactory Bulb. J Comp Neurol. 2016.

51. Hioki H, Nakamura H, Ma YF, Konno M, Hayakawa T, Nakamura KC, et al. Vesicular glutamate transporter 3-expressing nonserotonergic projection neurons constitute a subregion in the rat midbrain raphe nuclei. J Comp Neurol. 2010; 518(5):668–86. doi: 10.1002/cne.22237 PMID: 20034056

52. Fujiyama F, Furuta T, Kaneko T. Immunocytochemical localization of candidates for vesicular glutamate transporters in the rat cerebral cortex. J Comp Neurol. 2001; 435(3):379–87. PMID: 11406819

53. Hioki H, Fujiyama F, Taki K, Tomioka R, Furuta T, Tamamaki N, et al. Differential distribution of vesicular glutamate transporters in the rat cerebellar cortex. Neuroscience. 2003; 117(1):1–6. PMID: 12605886

54. Xu X, Roby KD, Callaway EM. Immunochemical characterization of inhibitory mouse cortical neurons: three chemically distinct classes of inhibitory cells. J Comp Neurol. 2010; 518(3):389–404. doi: 10.1002/cne.22229 PMID: 19950390

55. Rudy B, Fishell G, Lee S, Hjerling-Leffler J. Three groups of interneurons account for nearly 100% of neocortical GABAergic neurons. Dev Neurobiol. 2011; 71(1):45–61. doi: 10.1002/dneu.20853 PMID: 21154909

56. Hioki H, Okamoto S, Konno M, Kameda H, Sohn J, Kuramoto E, et al. Cell type-specific inhibitory inputs to dendritic and somatic compartments of parvalbumin-expressing neocortical interneuron. J Neurosci. 2013; 33(2):544–55. doi: 10.1523/JNEUROSCI.2255-12.2013 PMID: 23303934

57. Kawaguchi Y, Kubota Y. Physiological and morphological identification of somatostatin- or vasoactive intestinal polypeptide-containing cells among GABAergic cell subtypes in rat frontal cortex. J Neurosci. 1996; 16(8):2701–15. PMID: 8786446

58. Kawaguchi Y, Kubota Y. GABAergic cell subtypes and their synaptic connections in rat frontal cortex. Cereb Cortex. 1997; 7(6):476–86. PMID: 9276173

59. Pronneke A, Scheuer B, Wagener RJ, Mock M, Witte M, Staiger JF. Characterizing VIP Neurons in the Barrel Cortex of VIPcre/tdTomato Mice Reveals Layer-Specific Differences. Cereb Cortex. 2015; 25(12):4854–68. doi: 10.1093/cercor/bhv202 PMID: 26420784

60. Connor JR, Peters A. Vasoactive Intestinal Polypeptide-Immunoreactive Neurons in Rat Visual-Cortex. Neuroscience. 1984; 12(4):1027–44. PMID: 6384816

61. Zilles K, Hajos F, Csillag A, Kalman M, Sotonyi P, Schleicher A. Vasoactive intestinal polypeptide immunoreactive structures in the mouse barrel field. Brain Res. 1993; 618(1):149–54. PMID: 8402168

62. Hajos F, Zilles K, Zsarnovszky A, Sotonyi P, Gallatz K, Schleicher A. Modular distribution of vasoactive intestinal polypeptide in the rat barrel cortex: changes induced by neonatal removal of vibrissae. Neuroscience. 1998; 85(1):45–52. PMID: 9607701

63. Welker C. Microelectrode delineation of fine grain somatotopic organization of (SmI) cerebral neocortex in albino rat. Brain Res. 1971; 26(2):259–75. PMID: 4100672

64. Simons DJ. Response properties of vibrissa units in rat SI somatosensory neocortex. J Neurophysiol. 1978; 41(3):798–820. PMID: 660231

65. Chapin JK. Laminar differences in sizes, shapes, and response profiles of cutaneous receptive fields in the rat SI cortex. Exp Brain Res. 1986; 62(3):549–59. PMID: 3720884

66. Armstrong-James M, Fox K. Spatiotemporal convergence and divergence in the rat S1 "barrel" cortex. J Comp Neurol. 1987; 263(2):265–81. doi: 10.1002/cne.902630209 PMID: 3667981

67. Welker E, Armstrong-James M, Van der Loos H, Kraftsik R. The mode of activation of a barrel column: response properties of single units in the somatosensory cortex of the mouse upon whisker deflection. Eur J Neurosci. 1993; 5(6):691–712. PMID: 8261141

68. Kaneko T, Fujiyama F. Complementary distribution of vesicular glutamate transporters in the central nervous system. Neurosci Res. 2002; 42(4):243–50. PMID: 11985876

69. Fremeau RT Jr., Voglmaier S, Seal RP, Edwards RH. VGLUTs define subsets of excitatory neurons and suggest novel roles for glutamate. Trends Neurosci. 2004; 27(2):98–103. doi: 10.1016/j.tins.2003.11.005 PMID: 15102489

70. Kaneko T, Fujiyama F, Hioki H. Immunohistochemical localization of candidates for vesicular glutamate transporters in the rat brain. J Comp Neurol. 2002; 444(1):39–62. PMID: 11835181

71. Liguz-Lecznar M, Skangiel-Kramska J. Vesicular glutamate transporters VGLUT1 and VGLUT2 in the developing mouse barrel cortex. Int J Dev Neurosci. 2007; 25(2):107–14. doi: 10.1016/j.ijdevneu.2006.12.005 PMID: 17289331

72. Nakamura K, Hioki H, Fujiyama F, Kaneko T. Postnatal changes of vesicular glutamate transporter (VGluT)1 and VGluT2 immunoreactivities and their colocalization in the mouse forebrain. J Comp Neurol. 2005; 492(3):263–88. doi: 10.1002/cne.20705 PMID: 16217795

73. Nakamura K, Watakabe A, Hioki H, Fujiyama F, Tanaka Y, Yamamori T, et al. Transiently increased colocalization of vesicular glutamate transporters 1 and 2 at single axon terminals during postnatal development of mouse neocortex: a quantitative analysis with correlation coefficient. Eur J Neurosci. 2007; 26(11):3054–67. doi: 10.1111/j.1460-9568.2007.05868.x PMID: 18028110

74. Bayraktar T, Welker E, Freund TF, Zilles K, Staiger JF. Neurons immunoreactive for vasoactive intestinal polypeptide in the rat primary somatosensory cortex: morphology and spatial relationship to barrel-related columns. J Comp Neurol. 2000; 420(3):291–304. PMID: 10754503

75. Niwa H, Yamamura K, Miyazaki J. Efficient selection for high-expression transfectants with a novel eukaryotic vector. Gene. 1991; 108(2):193–9. PMID: 1660837

76. Klein RL, Meyer EM, Peel AL, Zolotukhin S, Meyers C, Muzyczka N, et al. Neuron-specific transduction in the rat septohippocampal or nigrostriatal pathway by recombinant adeno-associated virus vectors. Exp Neurol. 1998; 150(2):183–94. doi: 10.1006/exnr.1997.6736 PMID: 9527887

77. Paterna JC, Moccetti T, Mura A, Feldon J, Bueler H. Influence of promoter and WHV post-transcriptional regulatory element on AAV-mediated transgene expression in the rat brain. Gene Ther. 2000; 7(15):1304–11. doi: 10.1038/sj.gt.3301221 PMID: 10918501

78. Lipshutz GS, Gruber CA, Cao Y, Hardy J, Contag CH, Gaensler KM. In utero delivery of adeno-associated viral vectors: intraperitoneal gene transfer produces long-term expression. Mol Ther. 2001; 3(3):284–92. doi: 10.1006/mthe.2001.0267 PMID: 11273769

79. Yin DX, Zhu L, Schimke RT. Tetracycline-controlled gene expression system achieves high-level and quantitative control of gene expression. Anal Biochem. 1996; 235(2):195–201. doi: 10.1006/abio.1996.0112 PMID: 8833328

80. Gascon S, Paez-Gomez JA, Diaz-Guerra M, Scheiffele P, Scholl FG. Dual-promoter lentiviral vectors for constitutive and regulated gene expression in neurons. J Neurosci Methods. 2008; 168(1):104–12. doi: 10.1016/j.jneumeth.2007.09.023 PMID: 17983662

81. de Backer MW, Fitzsimons CP, Brans MA, Luijendijk MC, Garner KM, Vreugdenhil E, et al. An adeno-associated viral vector transduces the rat hypothalamus and amygdala more efficient than a lentiviral vector. BMC Neurosci. 2010; 11:81. doi: 10.1186/1471-2202-11-81 PMID: 20626877

82. Alexander GE, Crutcher MD. Functional architecture of basal ganglia circuits: neural substrates of parallel processing. Trends Neurosci. 1990; 13(7):266–71. PMID: 1695401

83. Fujiyama F, Sohn J, Nakano T, Furuta T, Nakamura KC, Matsuda W, et al. Exclusive and common targets of neostriatofugal projections of rat striosome neurons: a single neuron-tracing study using a viral vector. Eur J Neurosci. 2011; 33(4):668–77. doi: 10.1111/j.1460-9568.2010.07564.x PMID: 21314848

84. Markram H, Toledo-Rodriguez M, Wang Y, Gupta A, Silberberg G, Wu C. Interneurons of the neocortical inhibitory system. Nat Rev Neurosci. 2004; 5(10):793–807. doi: 10.1038/nrn1519 PMID: 15378039

85. Kubota Y. Untangling GABAergic wiring in the cortical microcircuit. Curr Opin Neurobiol. 2014; 26:7–14. doi: 10.1016/j.conb.2013.10.003 PMID: 24650498

86. Ascoli GA, Alonso-Nanclares L, Anderson SA, Barrionuevo G, Benavides-Piccione R, Burkhalter A, et al. Petilla terminology: nomenclature of features of GABAergic interneurons of the cerebral cortex. Nat Rev Neurosci. 2008; 9(7):557–68. doi: 10.1038/nrn2402 PMID: 18568015

87. Hioki H. Compartmental organization of synaptic inputs to parvalbumin-expressing GABAergic neurons in mouse primary somatosensory cortex. Anat Sci Int. 2015; 90(1):7–21. doi: 10.1007/s12565-014-0264-8 PMID: 25467527

88. Pfeffer CK, Xue M, He M, Huang ZJ, Scanziani M. Inhibition of inhibition in visual cortex: the logic of connections between molecularly distinct interneurons. Nat Neurosci. 2013; 16(8):1068–76. doi: 10.1038/nn.3446 PMID: 23817549

89. Lee S, Kruglikov I, Huang ZJ, Fishell G, Rudy B. A disinhibitory circuit mediates motor integration in the somatosensory cortex. Nat Neurosci. 2013; 16(11):1662–70. doi: 10.1038/nn.3544 PMID: 24097044

90. Pi HJ, Hangya B, Kvitsiani D, Sanders JI, Huang ZJ, Kepecs A. Cortical interneurons that specialize in disinhibitory control. Nature. 2013; 503(7477):521–4. doi: 10.1038/nature12676 PMID: 24097352

91. Fu Y, Tucciarone JM, Espinosa JS, Sheng N, Darcy DP, Nicoll RA, et al. A cortical circuit for gain control by behavioral state. Cell. 2014; 156(6):1139–52. doi: 10.1016/j.cell.2014.01.050 PMID: 24630718

92. Zhang S, Xu M, Kamigaki T, Hoang Do JP, Chang WC, Jenvay S, et al. Selective attention. Long-range and local circuits for top-down modulation of visual cortex processing. Science. 2014; 345(6197):660–5. doi: 10.1126/science.1254126 PMID: 25104383

93. Veinante P, Deschenes M. Single-cell study of motor cortex projections to the barrel field in rats. J Comp Neurol. 2003; 464(1):98–103. doi: 10.1002/cne.10769 PMID: 12866130

94. Wimmer VC, Bruno RM, de Kock CP, Kuner T, Sakmann B. Dimensions of a projection column and architecture of VPM and POm axons in rat vibrissal cortex. Cereb Cortex. 2010; 20(10):2265–76. doi: 10.1093/cercor/bhq068 PMID: 20453248

95. Ohno S, Kuramoto E, Furuta T, Hioki H, Tanaka YR, Fujiyama F, et al. A morphological analysis of thalamocortical axon fibers of rat posterior thalamic nuclei: a single neuron tracing study with viral vectors. Cereb Cortex. 2012; 22(12):2840–57. doi: 10.1093/cercor/bhr356 PMID: 22190433

96. Diamond ME, Armstrong-James M, Budway MJ, Ebner FF. Somatic sensory responses in the rostral sector of the posterior group (POm) and in the ventral posterior medial nucleus (VPM) of the rat thalamus: dependence on the barrel field cortex. J Comp Neurol. 1992; 319(1):66–84. doi: 10.1002/cne.903190108 PMID: 1592906

97. Petreanu L, Gutnisky DA, Huber D, Xu NL, O'Connor DH, Tian L, et al. Activity in motor-sensory projections reveals distributed coding in somatosensation. Nature. 2012; 489(7415):299–303. doi: 10.1038/nature11321 PMID: 22922646

98. Xu NL, Harnett MT, Williams SR, Huber D, O'Connor DH, Svoboda K, et al. Nonlinear dendritic integration of sensory and motor input during an active sensing task. Nature. 2012; 492(7428):247–51. doi: 10.1038/nature11601 PMID: 23143335

99. Hama H, Hioki H, Namiki K, Hoshida T, Kurokawa H, Ishidate F, et al. ScaleS: an optical clearing palette for biological imaging. Nat Neurosci. 2015; 18(10):1518–29. doi: 10.1038/nn.4107 PMID: 26368944

100. Hama H, Kurokawa H, Kawano H, Ando R, Shimogori T, Noda H, et al. Scale: a chemical approach for fluorescence imaging and reconstruction of transparent mouse brain. Nat Neurosci. 2011; 14(11):1481–8. doi: 10.1038/nn.2928 PMID: 21878933

101. Tainaka K, Kubota SI, Suyama TQ, Susaki EA, Perrin D, Ukai-Tadenuma M, et al. Whole-body imaging with single-cell resolution by tissue decolorization. Cell. 2014; 159(4):911–24. doi: 10.1016/j.cell.2014.10.034 PMID: 25417165

102. Susaki EA, Tainaka K, Perrin D, Kishino F, Tawara T, Watanabe TM, et al. Whole-brain imaging with single-cell resolution using chemical cocktails and computational analysis. Cell. 2014; 157(3):726–39. doi: 10.1016/j.cell.2014.03.042 PMID: 24746791

103. Chung K, Wallace J, Kim SY, Kalyanasundaram S, Andalman AS, Davidson TJ, et al. Structural and molecular interrogation of intact biological systems. Nature. 2013; 497(7449):332–7. doi: 10.1038/nature12107 PMID: 23575631

104. Yang B, Treweek JB, Kulkarni RP, Deverman BE, Chen CK, Lubeck E, et al. Single-cell phenotyping within transparent intact tissue through whole-body clearing. Cell. 2014; 158(4):945–58. doi: 10.1016/j.cell.2014.07.017 PMID: 25088144

105. Ke MT, Fujimoto S, Imai T. SeeDB: a simple and morphology-preserving optical clearing agent for neuronal circuit reconstruction. Nat Neurosci. 2013; 16(8):1154–61. doi: 10.1038/nn.3447 PMID: 23792946

106. Ke MT, Nakai Y, Fujimoto S, Takayama R, Yoshida S, Kitajima TS, et al. Super-Resolution Mapping of Neuronal Circuitry With an Index-Optimized Clearing Agent. Cell Rep. 2016; 14(11):2718–32. doi: 10.1016/j.celrep.2016.02.057 PMID: 26972009

107. Erturk A, Becker K, Jahrling N, Mauch CP, Hojer CD, Egen JG, et al. Three-dimensional imaging of solvent-cleared organs using 3DISCO. Nat Protoc. 2012; 7(11):1983–95. doi: 10.1038/nprot.2012.119 PMID: 23060243

108. Renier N, Wu Z, Simon DJ, Yang J, Ariel P, Tessier-Lavigne M. iDISCO: a simple, rapid method to immunolabel large tissue samples for volume imaging. Cell. 2014; 159(4):896–910. doi: 10.1016/j.cell.2014.10.010 PMID: 25417164

109. Pan C, Cai R, Quacquarelli FP, Ghasemigharagoz A, Lourbopoulos A, Matryba P, et al. Shrinkage-mediated imaging of entire organs and organisms using uDISCO. Nat Methods. 2016.